Available online at www.sciencedirect.com
ScienceDirect
International Journal of Multiphase Flow 33 (2007) 1153–1171
International Journal of Multiphase Flow
www.elsevier.com/locate/ijmulflow

Surfactant effects on the Rayleigh instability in capillary tubes – non-ideal systems

D. Campana [a,b,*], F.A. Saita [a]

[a] *Instituto de Desarrollo Tecnológico para la Industria Química (INTEC) – Universidad Nacional del Litoral – CONICET, Güemes 3450, S3000GLN, Santa Fe, Argentina*

[b] *Facultad de Ingeniería – Universidad Nacional de Entre Ríos, Ruta Prov. 11 Km.10 – C.C. 57, Suc. 3, E3100, Paraná, Entre Ríos, Argentina*

Received 30 October 2006; received in revised form 20 February 2007

Abstract

In a previous work, the instability of a liquid film deposited on the inner walls of a capillary under the presence of insoluble surfactant was analyzed; for that purpose the surface tension was related to the interfacial concentration of surfactant by a linear equation. In general, that assumption is valid when just trace amounts of surfactant are present. The present work extends previous analysis by considering a non-linear surface equation of state derived from the Frumkin adsorption isotherm. This equation of state account not only for the existing quantities of surfactant but also for non-ideal interactions between adsorbed molecules. Except for the equation of state, both the model and the numerical technique employed do not differ from those used in the preceding work. The new predictions here presented show that a linear surface equation of state gives reasonable results for strong surfactants. However, the action of weaker surfactants strongly depends on other parameters: the initial concentration and the type and strength of interaction between adsorbed molecules. Thus, the use of a linear equation of state in these circumstances might give erroneous results.

Keywords: Rayleigh instability; Surfactants; Frumkin kinetics; Numerical analysis

1. Introduction

Annular liquid films deposited either on the inner or outer face of a capillary tube, are known to be unstable to axially symmetric surface perturbations of wavelengths of the order of the interfacial perimeter. A uniform film, wetting the inner face of a capillary tube, naturally evolves toward regularly spaced collars that eventually will break up into liquid lenses if the initial film is thick enough. On the other hand, if the film is deposited on a filament (or on the outer face of a capillary), the instability will form regularly spaced drops or pearls.

* Corresponding author. Address: Instituto de Desarrollo Tecnológico para la Industria Química (INTEC) – Universidad Nacional del Litoral – CONICET, Güemes 3450, S3000GLN, Santa Fe, Argentina. Tel.: +54 0 342 455 9175 76 77; fax: +54 0 342 455 0944.
E-mail address: dcampana@ceride.gov.ar (D. Campana).
URLs: http://www.intec.ceride.gov.ar (D. Campana, F.A. Saita), http://www.bioingenieria.edu.ar (D. Campana).

0301-9322/$ - see front matter © 2007 Elsevier Ltd. All rights reserved.
doi:10.1016/j.ijmultiphaseflow.2007.05.006

Following the lines of Rayleigh's pioneer work (Rayleigh, 1879), earlier studies performed linear stability analysis; among them we might mention those of Weber (1931), Tomotika (1935), and particularly Goren (1962) who determined the unstable modes with the largest growth rate when the Reynolds number is equal to zero and infinity, respectively.

Since this phenomenon has close connections with several industrial and biological processes, particularly with a disease known as Respiratory Distress Syndrome (RDS) that commonly occurs in premature neonates, it has received renewed attention since the 1980s. At that point the objective pursued was to establish the minimum film thickness needed to produce the lenses that occlude the capillary passage, and the time needed to do it—i.e. the so-called "closure time". Employing interfacial evolution equations, which were derived on the assumption that lubrication approximation applies, these results were obtained first for pure liquids (Hammond, 1983; Gauglitz and Radke, 1988) and then for liquids with insoluble surfactants (Otis et al., 1993; Halpern and Grotberg, 1993).

The effects produced by surfactants on film instability might be crucial; in that regard, we recall that a surfactant deficiency is precisely the factor that triggers RDS. Thus, a more elaborate two-dimensional model was employed to assess the quality of the predictions based on the lubrication approximation (Campana et al., 2004). The results showed that interfacial evolution equations underestimate closure times, being this underestimation much more significant when surfactants are present; i.e. when flow equations become coupled with mass transport equations and the interfacial tension changes locally giving rise to Marangoni effect. The conclusion was that predictions of simple one-dimensional models become more unreliable as the system to be modeled shows more non-linear contributions.

The analysis for insoluble surfactant performed by Campana et al. (2004) was extended to take into account for soluble ones (Campana and Saita, 2006); however, in both cases just a linear relation between surface tension and interfacial concentration of surfactant (equation of state) was considered. Though this approach is valid just for very dilute concentrations, or for small departures from equilibrium, it has been widely employed by several authors (Halpern and Grotberg, 1993; Jensen and Grotberg, 1993; Kwak and Pozrikidis, 2001; Otis et al., 1993).

The present work aims at establishing how the Rayleigh instability is affected when there is interaction between molecules of adsorbed solute, and when the concentration of surfactant is far from dilute. For that purpose, we will employ non-linear equations of state stemming from Frumkin and Langmuir adsorption isotherms; and, in order to focus our attention in the non-ideal effects we will only consider situations where surfactants can be regarded as insoluble solutes.

The presentation is arranged in the following order: the next section presents the mathematical formulation of the problem where the set of governing equations and appropriate boundary conditions are made explicit; also, special attention is paid to the surface equation of state and brief reference is made to the numerical technique employed. Then, before presenting the predictions of the model, a short section is devoted to define the reference system adopted and to compare the behavior of the non-linear equation of state with the linear one. In the central section, computed predictions show how the concentration of surfactants and the non-ideal behavior bear upon the liquid film instability in capillaries; finally, the last section summarizes the relevant conclusions.

2. Mathematical formulation

2.1. The flow problem and the interfacial mass balance

The flow problem as well as the interfacial mass balance has already been clearly described by Campana et al. (2004); therefore, just a summary of the governing equations and boundary conditions is given here.

Fig. 1 is a schematic representation of the problem showing a gas phase surrounded by a thin liquid film, which is assumed Newtonian and incompressible of constant viscosity μ and density ρ. An insoluble surfactant is adsorbed at the gas–liquid interface; when the system is at rest the uniform interfacial concentration is Γ_0 and the corresponding surface tension is σ_0. The unperturbed liquid film wets the inner walls of a capillary of radius (a), and the gas liquid interface is located at a distance (b) from the capillary axis, thus the relative film thickness F is $(a - b)/a$.

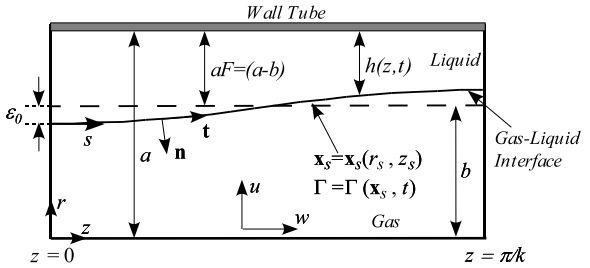

Fig. 1. Schematic representation of the flow domain. Variables and magnitudes are indicated in their dimensionless form, except for a and b.

The flow problem is governed by the equations of motion—continuity and momentum—that, according to the moving mesh adopted for this problem and considering dimensionless variables, can be written as follows:

$$\nabla \cdot \mathbf{v} = 0 \tag{1}$$

$$Re\left[\left(\frac{\partial \mathbf{v}}{\partial t}\right)_{\mathbf{x}} + (\mathbf{v} - \dot{\mathbf{x}}) \cdot \nabla \mathbf{v}\right] = \nabla \cdot \mathbf{T}$$
$$\mathbf{T} = -p/Ca\mathbf{I} + (\nabla \mathbf{v} + \nabla \mathbf{v}^{\mathrm{T}}) \tag{2}$$

In the equations just shown, we have used the capillary radius (a) as the unit of measure for lengths, and the quantities $\sigma_0 F^3/\mu$ and σ_0/a as unit of measure for velocities and pressure, respectively (Hammond, 1983). The components of the stress tensor $\mathbf{T}$ are measured in terms of $\sigma_0 F^3/a$ and the time scale is $a\mu/\sigma_0 F^3$. The modified Reynolds number is $Re = a\rho\sigma_0 F^3/\mu^2$, the Capillary number is $Ca = F^3$, and the term $(\dot{\mathbf{x}} \cdot \nabla \mathbf{v})$ considers the radial motion of the nodes (see Campana et al., 2004). The interface is parameterized by h, which is the distance to the capillary wall scaled with the capillary radius (a). Since the interfacial shape $h(z,t)$ is unknown, the equation set is completed with the so-called kinematics condition establishing that the gas–liquid interface is a material surface

$$(\mathbf{n} \cdot \mathbf{v})|_s = \mathbf{n} \cdot \dot{\mathbf{x}}_s \tag{3}$$

where the subscript (s) indicates that the terms are evaluated at the interface.

The unstable motion sets off by perturbing the interfacial shape with a sinusoidal wave of amplitude ε_0 and wave-number k

$$h(z,0) = F[1 + \varepsilon_0 \cos(kz)] \tag{4}$$

Since we impose a periodic perturbation, we use a problem domain that just extends half wavelength in the z-direction; thus, we employed symmetry conditions at both ends of the domain, i.e.

$$w = 0; \quad \frac{\partial u}{\partial z} = 0 \quad \text{and} \quad \frac{\partial h}{\partial z} = 0 \quad \text{at } z = 0 \quad \text{and} \quad z = \pi/k \tag{5}$$

On solid walls the usual non-slip condition is imposed ($u = w = 0$); finally, on the interface the stress balance in dimensionless form is given by

$$\mathbf{n} \cdot \mathbf{T} = \frac{1}{Ca}[\sigma\kappa\mathbf{n} + \nabla_s \sigma] \tag{6}$$

where κ is twice the mean interfacial curvature, ∇_s is the interfacial gradient operator and σ is the local surface tension. Eq. (6) was obtained on the assumption that the gas phase is inviscid and its pressure is arbitrarily defined as zero; additionally, interfacial viscous effects are neglected and the tangential stresses at the interface are produced by surface tension gradients, exclusively.

The surface tension depends upon the local concentration of surfactant, and this is how the flow and mass transport problems are coupled. In this work, we consider just insoluble surfactant (see Section 3.1); consequently, the mass transfer problem reduces to the interfacial mass balance of solute given by the following dimensionless equation (Edwards et al., 1991; Wong et al., 1996):

$$\left(\frac{\partial \Gamma}{\partial t}\right)\bigg|_{\mathbf{x}_s} - \dot{\mathbf{x}}_s \cdot \nabla_s \Gamma = -\Gamma v_{(\mathbf{n})}(\nabla_s \cdot \mathbf{n}) - \nabla_s \cdot (\Gamma \mathbf{v}_s) + \frac{1}{Pe_s}\nabla_s^2 \Gamma \tag{7}$$

The first term in Eq. (7) stands for the time derivative of the concentration of solute at fixed surface coordinates—which are moving with respect to a fixed frame (r, z). The third and four terms represent the transport by normal and tangential convection, respectively, and the last term takes into account the transport by surface diffusion. $Pe_s = a\sigma_0 F^3/\mu D_s$ is the interfacial Peclet number and D_s is the interfacial diffusion coefficient which is assumed constant and isotropic. The dimensionless interfacial concentration Γ is scaled with the uniform initial interfacial concentration Γ_0; therefore, the initial condition to be used in Eq. (7) is $\Gamma(\mathbf{x}_s, t = 0) = 1$. At both extremes of the interface ($s = 0$ and $s = s_f$ which have the axial coordinates $z = 0$ and $z = \pi/k$, respectively) we impose symmetry conditions

$$\mathbf{t} \cdot \nabla_s \Gamma = \mathrm{d}\Gamma/\mathrm{d}s = 0, \quad \text{at } s = 0 \text{ and } s = s_f \tag{8}$$

This boundary condition together with the first boundary condition stated in (5), guarantees that there is no transport of solute at both ends of the interface.

2.2. Equation of state

The Gibbs thermodynamics relation is used to find the equation of state that connects surface tension with the interfacial concentration of surfactant, that relation is given in Eq. (9) where the asterisks indicate dimensional quantities.

$$\mathrm{d}\sigma^* = -R_g T \Gamma^* \,\mathrm{d}[\ln C_s^*] = -R_g T \Gamma^* \frac{1}{C_s^*}\,\mathrm{d}C_s^* \tag{9}$$

In Eq. (9) R_g is the universal gas constant, T is the absolute temperature and C_s^* is the bulk concentration of surfactant just at the interface. On the assumption that an instantaneous local equilibrium between C_s^* and Γ^* exists, an adsorption isotherm can be employed to substitute one of these variables. In this work, we use the Frumkin isotherm (see, Edwards et al., 1991) that has the following expression:

$$K_F C_s^* = \frac{\Gamma^*}{\Gamma_\infty - \Gamma^*} \mathrm{e}^{-A\Gamma^*/\Gamma_\infty} \tag{10}$$

where $K_F = k_a/(k_d \Gamma_\infty)$, being k_a and k_d the kinetic constants of adsorption and de-sorption, respectively, and Γ_∞ is the maximum attainable interfacial concentration of solute. The parameter A measures the non-ideal behavior of the adsorbed solute; if $A > 0$ the adsorbed molecules of surfactant interact in a cohesive manner, while they do in a repulsive way if $A < 0$.

When Eq. (10) is introduced into Eq. (9) and the resulting expression is integrated between a reference state $(\sigma_{\mathrm{ref}}, \Gamma_{\mathrm{ref}})$ and some arbitrary state (σ^*, Γ^*), the equation of state for the Frumkin isotherm is obtained.

$$\sigma^* = \sigma_{\mathrm{ref}} + R_g T \Gamma_\infty \left[\ln\left(\frac{\Gamma_\infty - \Gamma^*}{\Gamma_\infty - \Gamma_{\mathrm{ref}}}\right) + \frac{A}{2\Gamma_\infty^2}\left(\Gamma^{*2} - \Gamma_{\mathrm{ref}}^2\right)\right] \tag{11}$$

If the initial state (σ_0, Γ_0) is chosen as the reference state, the dimensionless form of Eq. (11) is

$$\sigma = 1 + \beta \widetilde{\Gamma}_\infty \left[\ln\left(\frac{\widetilde{\Gamma}_\infty - \Gamma}{\widetilde{\Gamma}_\infty - 1}\right) + \frac{A}{2\widetilde{\Gamma}_\infty^2}\left(\Gamma^2 - 1\right)\right] \tag{12}$$

being $\beta = R_g T \Gamma_0/\sigma_0$.

Linearization of Eq. (12) about $\Gamma = 1$ gives

$$\sigma = 1 - E(\Gamma - 1), \quad E = -\left(\frac{\partial \sigma}{\partial \Gamma}\right)_{\Gamma=1} = \beta \widetilde{\Gamma}_\infty \left[\frac{1}{\widetilde{\Gamma}_\infty - 1} - \frac{A}{\widetilde{\Gamma}_\infty^2}\right] \tag{13}$$

E is the dimensionless elastic parameter, which is equal to E_0/σ_0, where E_0 is the Gibbs elasticity (see Edwards et al., 1991). It must be noticed that for very dilute concentrations (i.e. $\widetilde{\Gamma}_\infty \to \infty$) we recover the equation

$\sigma = 1 - \beta(\Gamma - 1)$ employed in previous papers (Campana et al., 2004; Campana and Saita, 2006). In the remaining of this work, we will refer to results obtained with this equation as the results of the linear equation of state.

The system of equations (Eqs. (1), (2), (3), (7) and (12)) with appropriate initial (Eq. (4)) and boundary conditions was transformed into an algebraic non-linear analogue with the aid of the finite element technique; a finite difference scheme coupled with a second order predictor-corrector procedure was used to march in time. We employed mixed interpolation, i.e. polynomials of different degrees were used to approximate velocities and pressures; we chose biquadratic basis functions for velocities and bilinear basis functions for pressure. Newton iteration was used at each time step to determine all variables simultaneously, including those used to locate the free surface. The numerical procedures, as well as the results validating the computational code employed, were wholly described elsewhere (Campana et al., 2004); thus, we will not give more details about these topics here.

The non-linear equation of state (Eq. (12)) allows us to determine how the concentration of surfactant ($\widetilde{\Gamma}_\infty$) and the non-ideal interfacial behavior represented by a non-zero value of A, act upon the speed of the instability. The results of the linear model ($\sigma = 1 - \beta(\Gamma - 1)$) are used as a baseline to quantify the errors committed when conditions of dilute concentrations and small departures from equilibrium are assumed. This analysis is undertaken in the following sections.

3. Preliminaries

3.1. Reference system

In order to start the analysis we must define a reference system by assuming appropriate values for the dimensionless parameters appearing in the governing equations. Then, the concentration of surfactant and the value of A, will be varied about those used in the base case to analyze the effects they produce on the speed of the instability. We must also adopt values for several other physical parameters like maximum interfacial concentration of solute (Γ_∞), reference surface tension (σ_0), etc. Table 1 summarizes for each one of these parameters, their usual range and the value adopted in this work; the data were taken from several sources and an important one was the work of Chang and Franses (1995). Table 2 shows the values chosen for the relevant dimensionless parameters of the problem.

Table 1
Values of the physical magnitudes: usual range and value adopted

Physical magnitude	Range of values	Selected value
Γ_∞ [mol/m^2]	10^{-6} –10^{-5}	5×10^{-6}
Γ_0 [mol/m^2]	–	2×10^{-6}
A	−2 to 2	0
D_s [m^2/s]	10^{-10}–10^{-8}	10^{-9}
σ_{ref} [N/m]	$[15–75]\times10^{-3}$	40×10^{-3}
μ [Pa s]	10^{-3}–0, 1	10^{-2}
a [m]	10^{-4}–10^{-3}	5×10^{-4}
ρ [kg/m^3]	800–1400	1100
T [K]	—	300

Table 2
Value of the dimensionless parameters

$F = (a-b)/a$	0.18
$Re = \rho\sigma_{ref}aF^3/\mu^2$	$1{,}28 \approx 1$
$Ca = F^3$	5.8×10^{-3}
$\widetilde{\Gamma}_\infty = \Gamma_\infty/\Gamma_0$	2.5
$Pe_s = \sigma_{ref}aF^3/(\mu D_s)$	$11664 \approx 10^4$
$\beta = R_g T\Gamma_0/\sigma_{ref}$	$0.15 \approx 0.1$
$k^{max} = 2\pi a/\lambda$	0.8537 (Goren, 1962)

Since this paper focuses on how the instability process is affected by non-ideal surfactants acting at interfacial concentrations far from dilute, for the sake of simplicity we will consider situations where surfactants can be regarded as insoluble. Campana and Saita (2006) showed that if the relative amount of surfactant present in the bulk is low—situation characterized by the dimensionless parameter $K = \Gamma_0/(aC_0) \gg 1$—the system rapidly approaches the results obtained for a totally insoluble surfactant ($K \to \infty$), provided that the bulk Peclet number ($Pe = F^3\sigma_0 a/(D\mu)$) is large enough, so that the product (KPe) is larger than one. Predictions already presented by Campana and Saita (2006) showed that for the values of the parameters employed in the present work, that condition is attained when $K \geqslant 10$.

We are going to evaluate the effects produced by both $\widetilde{\Gamma}_\infty$ and A on the speed of the instability by measuring the values of closure time. The closure time is the time elapsed between the instant at which the annular film is perturbed, and the instant at which the growing liquid collars reach the capillary axis producing liquid lenses that disconnect the gas phase. The experimental work of Chang and Franses (1995) reported values for the parameter A varying between 0 and 2; positive values of A indicate that the adsorbed molecules of surfactant interact in a cohesive manner. In this analysis, we also use a negative value of A to include the case of repulsive interactions; therefore, we will show predictions for values of A equal to 2, -2 and 0 to consider the three possible cases: cohesive, repulsive and non-existing interactions, respectively. For that purpose, it is convenient to observe first how the equation of state behaves when the values of $\widetilde{\Gamma}_\infty$ and A are changed.

3.2. Effect of $\widetilde{\Gamma}_\infty$ and A on the equation of state

The equation of state chosen (Eq. (12)) can be written as

$$\sigma = 1 + \beta\Im(\widetilde{\Gamma}_\infty, A, \Gamma) \tag{14}$$

with

$$\Im(\widetilde{\Gamma}_\infty, A, \Gamma) = \widetilde{\Gamma}_\infty \left[\ln\left(\frac{\widetilde{\Gamma}_\infty - \Gamma}{\widetilde{\Gamma}_\infty - 1}\right) + \frac{A}{2\widetilde{\Gamma}_\infty^2}\left(\Gamma^2 - 1\right) \right] \tag{15}$$

When $(1 - \Gamma)$ is subtracted from Eq. (15), the resulting function can be thought of as the deviation from the ideal case since for highly dilute systems (i.e. $\widetilde{\Gamma}_\infty \to \infty$) and regardless of the value of A, $\Im(\widetilde{\Gamma}_\infty, A, \Gamma)$ tends to $(1 - \Gamma)$.

Fig. 2 illustrates the behavior of $\Im(\widetilde{\Gamma}_\infty, A, \Gamma)$ for the three values of A just indicated and also for three values of $\widetilde{\Gamma}_\infty$; they are 1.3, 2.5 and 25 corresponding to high, intermediate and low concentration of solute, respectively. In addition, the linear behavior, that is attained when $\widetilde{\Gamma}_\infty \to \infty$, is portrayed.

Fig. 2(a) shows the results for the lowest concentration of solute here considered ($\widetilde{\Gamma}_\infty = 25$); in this condition, the system behaves rather similarly for the three values of A. In all cases, none of the curves departs too much from the straight line $(1 - \Gamma)$ suggesting that the linear approximation employed in previous works is a good choice for dilute systems. However, when a tenfold increase in the concentration of solute is assumed ($\widetilde{\Gamma}_\infty = 2.5$), results depicted in Fig. 2(b) indicate that important departures from the linear case are occurring; this trend heightens as the concentration of solute approaches the maximum feasible concentration (see Fig. 2(c)). Fig. 2 also evidence that a repulsive interaction between molecules of adsorbed surfactants results into a system with stronger elastic effects; clearly, the value of E given by $-\beta(\partial\Im/\partial\Gamma)_{\Gamma=1}$ increases as A becomes more negative.

4. Computed predictions

In a preceding paper (Campana and Saita, 2006), we pointed out that the successive interfacial shapes adopted by an unstable liquid film of a given thickness and physical properties, do not depend on the presence of surfactants. The action of surfactants is to delay the instability process and the extent of retardation will depend upon the surfactant strength. Therefore, we can directly relate the interfacial configuration with the progress of the instability, and to use the times required to reach a given configuration to make relative com-

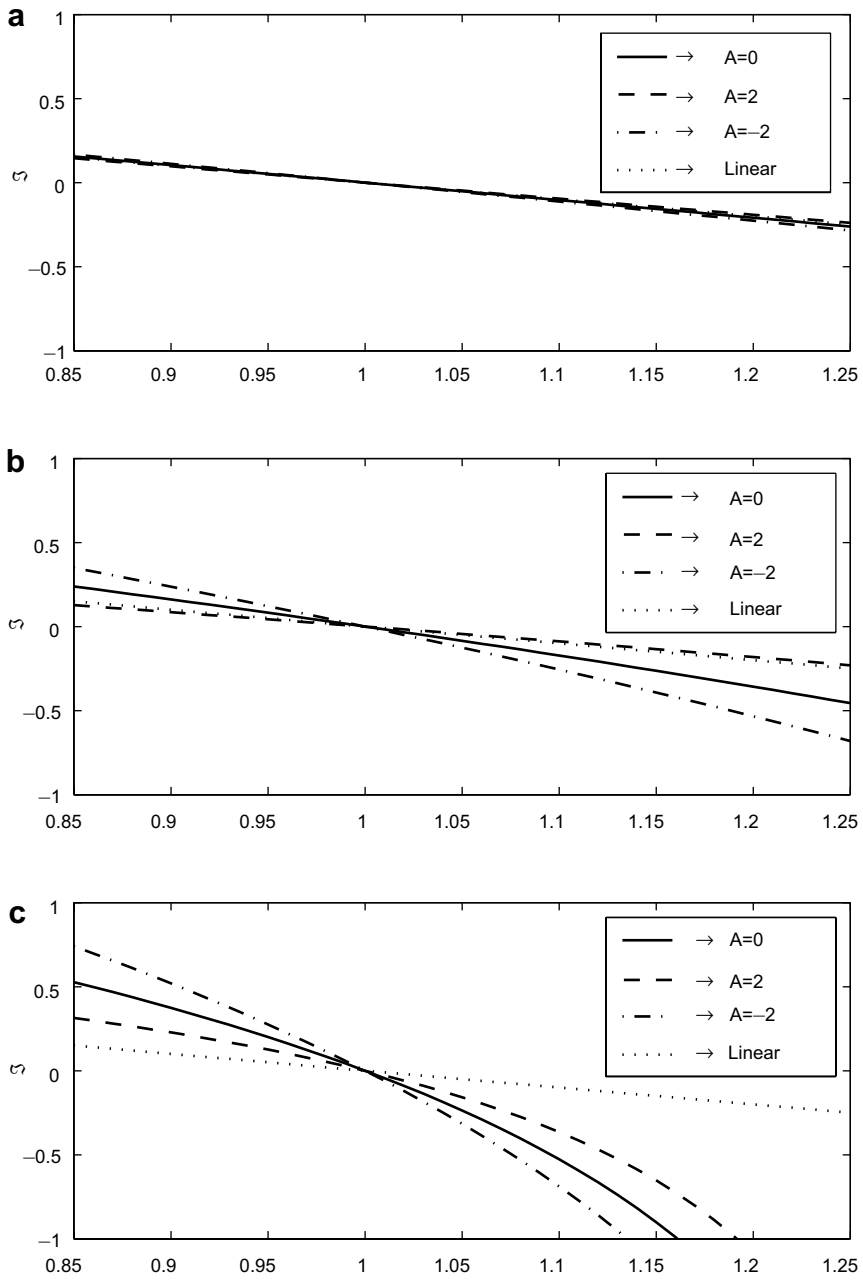

Fig. 2. Predictions of Eq. (15) for three values of A versus interfacial concentration of surfactant. (a) $\widetilde{\Gamma}_\infty = 25$, (b) $\widetilde{\Gamma}_\infty = 2.5$ and (c) $\widetilde{\Gamma}_\infty = 1.3$. The limit $(1 - \Gamma)$ of Eq. (15) is also shown.

parisons between different surfactants. This strategy will be used here to evaluate how the surfactant strength depends upon its concentration and its non-ideal behavior.

Fig. 3 shows for five successive instants of time the shapes adopted by a liquid film whose relative initial thickness (F) is 0.18; with the addition of the interfacial shape corresponding to closure, these are the interfacial configurations to be used throughout this work.

Fig. 4 depicts the dimensionless closure time versus A for a liquid film characterized by $\beta = 0.01$ and the parameter values summarized in Table 2. The results are presented for four different concentrations; since

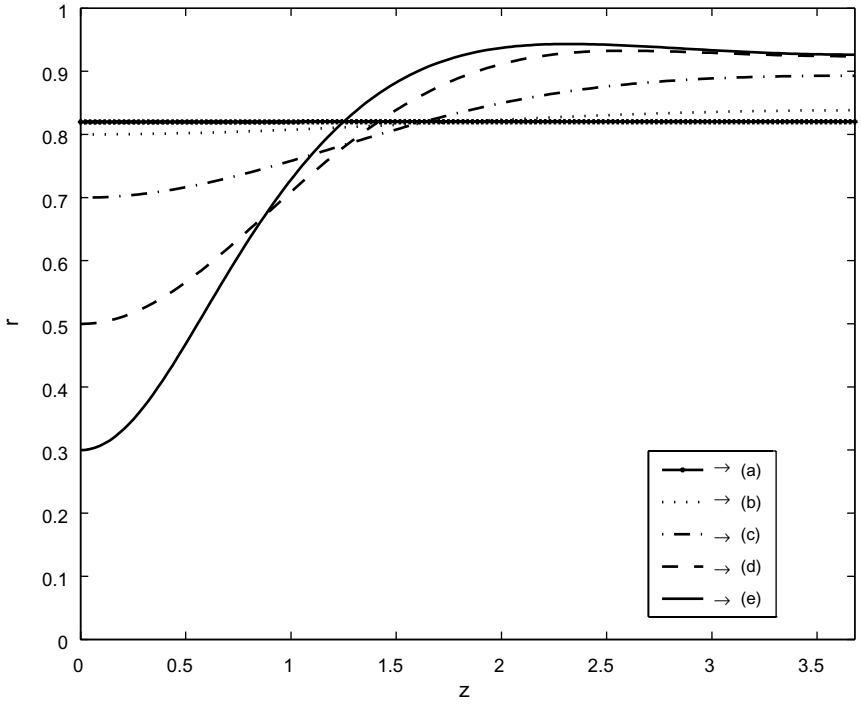

Fig. 3. Interfacial profiles depicting the five stages of the instability used throughout this work to compare different systems.

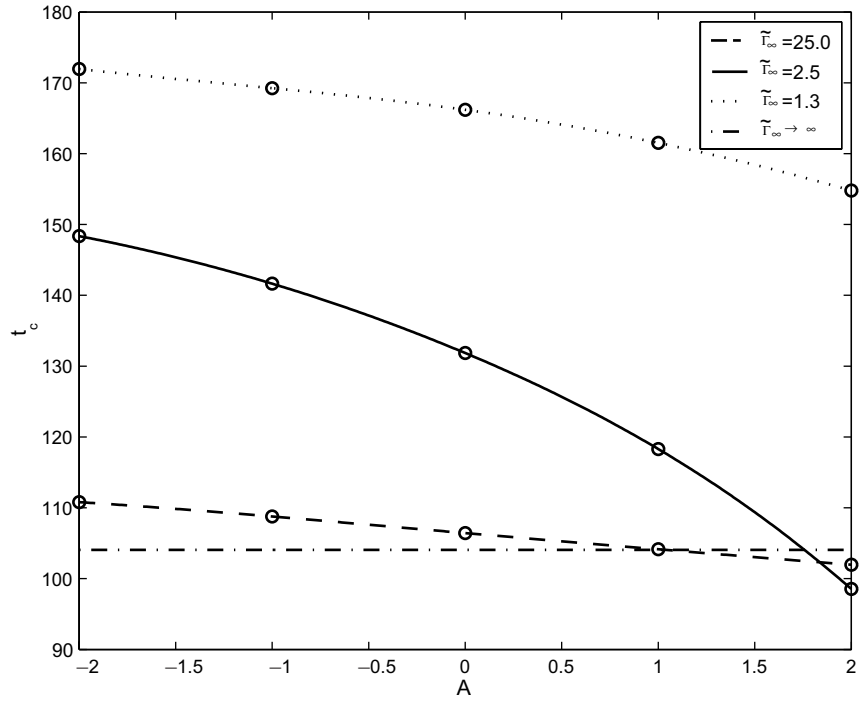

Fig. 4. Closure times versus A for different values of initial concentration. The parameters of the system are those of the reference case with $\beta = 0.01$; the closure time of the linear approximation is 104.06.

the most diluted system contains just trace of surfactant ($\widetilde{\Gamma}_\infty \to \infty$), it follows a linear equation of state and closure times do not depend on A.

We are going to examine the results of Fig. 4 in more detail; first, we will study the effects of solute concentration ($\widetilde{\Gamma}_\infty$) considering an ideal system ($A = 0$) and then we will vary the values of A for a certain value of $\widetilde{\Gamma}_\infty$. To understand how these parameters change the closure times we will examine the behavior of the following variables: tangential interfacial velocities ($V_s = \mathbf{v}_s \cdot \mathbf{t}$), interfacial concentrations (Γ), and tangential or Marangoni stresses (T_{ns}). In addition, we will look at the different terms appearing in the interfacial mass balance equation (Eq. (7)).

4.1. Ideal system ($A = 0$)

Fig. 5 portrays for three values of the initial concentration of surfactant ($\widetilde{\Gamma}_\infty$), how the tangential velocities change along the interface for each one of the five interfacial configurations shown in Fig. 3. These results are for system with an ideal interface, and the dimensionless times pertaining at each concentration are indicated in the corresponding insets. Clearly, as the solute concentration increases (from top to bottom), the whole instability process slows down as it is indicated by the corresponding sets of the dimensionless time; these results are in agreement with the trend for the closure times already shown in Fig. 4.

The values of interfacial tangential velocities shown at the top of Fig. 5 ($\widetilde{\Gamma}_\infty = 25$) are negative indicating—according to the positive direction defined for the surface tangential vector in Fig. 1—that the liquid at the interface, or close to it, is moving from right lo left, i.e. following the bulk motion. When the solute concentration is augmented to 2.5, the tangential velocities are still mostly negative; however, their magnitudes are smaller than before. For even larger concentrations of surfactant ($\widetilde{\Gamma}_\infty = 1.3$), the bottom of Fig. 5 shows that the interfacial tangential velocities has changed direction and now is positive in the region where the liquid collar is growing. It is evident that the interfacial velocity increasingly resists the bulk motion and delays the instability, as the adsorbed surfactant becomes more concentrated.

The observed changes in the tangential velocities are directly related to the tangential stresses acting at the interface. The tangential component of the traction vector (Eq. (6)) gives the tangential stress at the interface

$$T_{ns} = \mathbf{n} \cdot \mathbf{T} \cdot \mathbf{t} = Ca^{-1}(\nabla_s \sigma \cdot \mathbf{t}) \tag{16}$$

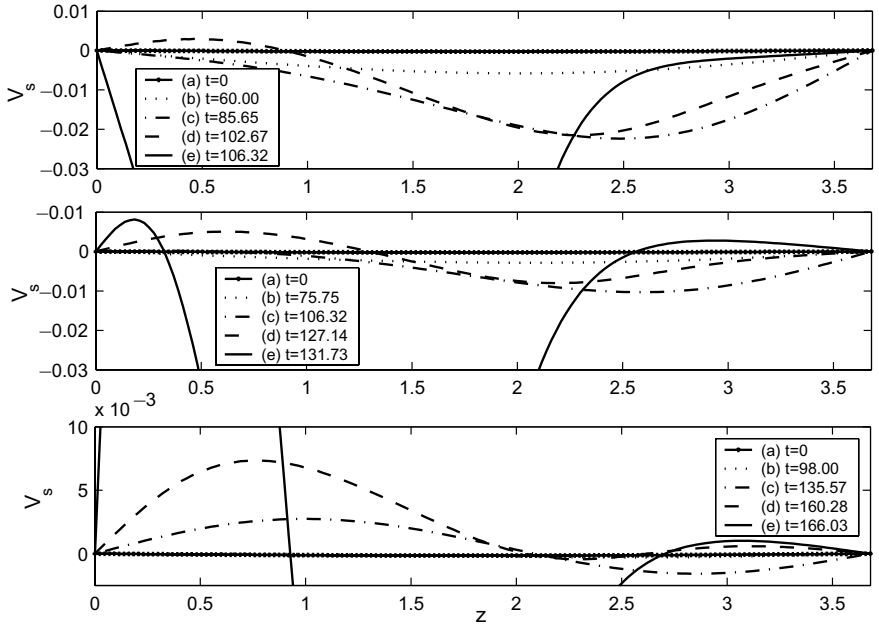

Fig. 5. Profiles of interfacial tangential velocities for the five interfacial configurations shown in Fig. 3. The system is the reference case with $A = 0$; from top to bottom the values of $\widetilde{\Gamma}_\infty$ are 25, 2.5 and 1.3.

and, given the axial symmetry, Eq. (16) can be written as

$$T_{ns} = Ca^{-1}\left(\frac{\partial\sigma}{\partial\Gamma}\right)\frac{\mathrm{d}\Gamma}{\mathrm{d}s} \tag{17}$$

Considering Eqs. (14) and (15), we obtain

$$\left(\frac{\partial\sigma}{\partial\Gamma}\right) = \beta\frac{\partial\left[\Im(\widetilde{\Gamma}_\infty, A, \Gamma)\right]}{\partial\Gamma} = -\beta\widetilde{\Gamma}_\infty\left[\frac{1}{\widetilde{\Gamma}_\infty - \Gamma} - \frac{A\Gamma}{\widetilde{\Gamma}_\infty^2}\right] \tag{18}$$

when Eq. (18) is introduced into Eq. (17) we finally get

$$T_{ns} = -\beta Ca^{-1}\left[\frac{\widetilde{\Gamma}_\infty}{\widetilde{\Gamma}_\infty - \Gamma} - \frac{A\Gamma}{\widetilde{\Gamma}_\infty}\right]\frac{\mathrm{d}\Gamma}{\mathrm{d}s} \tag{19}$$

Fig. 6 shows that the interfacial tangential stresses are positive and they increase with the concentration of surfactant; ultimately, they produce the changes just observed in the interfacial velocities and they are responsible for the lengthier evolution of the instability. Fig. 7 portrays the profiles of the interfacial concentration of solute; it is interesting to notice that the term $(-\mathrm{d}\Gamma/\mathrm{d}s)$ diminishes when the amount of adsorbed surfactant increases; i.e. as we go from top to bottom in Fig. 7, the Marangoni stresses produce a solute distribution that is closer to equilibrium and the interfacial concentration gradients are smoothed out. Therefore, according to Eq. (19) the term between brackets must produce the growth of the tangential stresses.

In the analysis of a rather similar situation Wong et al. (1999) provided an alternative explanation. These authors argued that the interfacial concentration of surfactant becomes uniform (see Fig. 7) when Marangoni forces prevail ($Ma = \beta/Ca \to \infty$); then, the interfacial mass balance directly prescribes the interfacial velocity $\mathbf{v}_s$. In this way, if the normal convection tend to concentrate solute in the lobe, the mass balance dictates that the tangential convection must extract surfactant out of this region and sets the direction of the interfacial velocity away from the lobe.

The effect of the tangential stresses shown in Fig. 6 can be better quantified by computing the total force they exert on the interface in the axial direction, i.e.

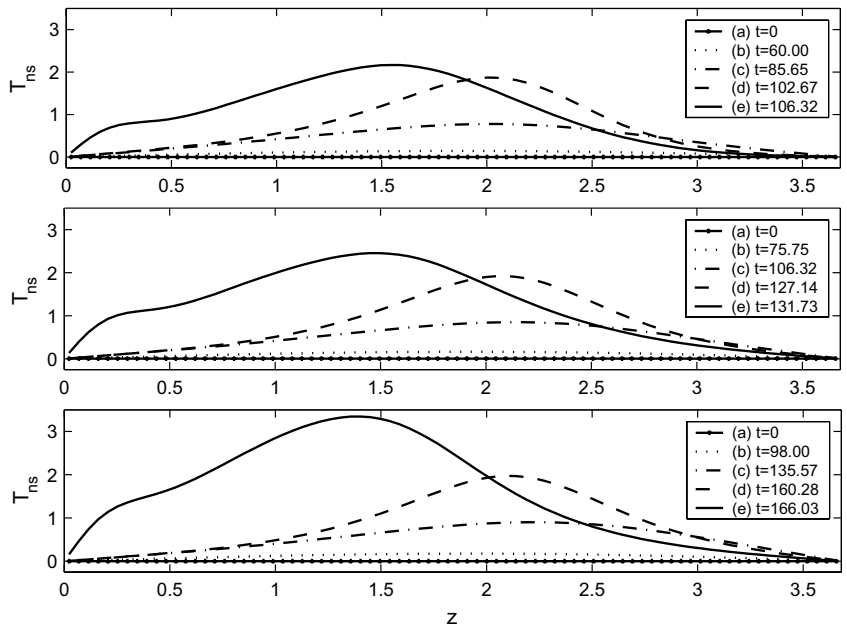

Fig. 6. Profiles of interfacial tangential stresses (as in Fig. 5).

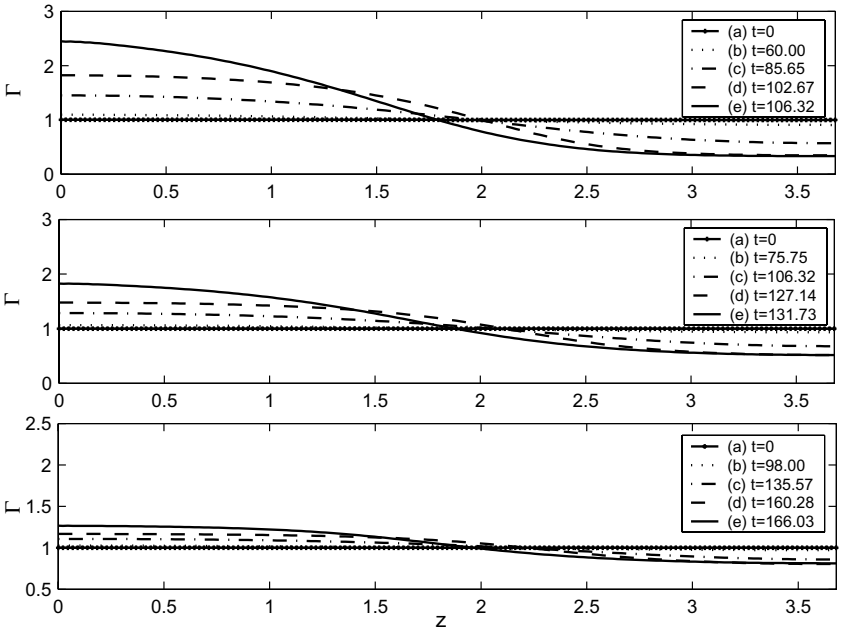

Fig. 7. Profiles of interfacial concentrations of surfactant (as in Fig. 5).

$$F_z = 2\pi \int_0^{s_f} (T_{ns}\mathbf{t} \cdot \mathbf{e_z}) r_s \, \mathrm{d}s \tag{20}$$

Table 3 summarizes these values for the three cases just analyzed and for the five interfacial configurations corresponding to each case; they confirm that F_z increases as the concentration of surfactant increases—that is as $\widetilde{\Gamma}_\infty$ diminishes.

Fig. 7 indicates that Γ changes significantly with $\widetilde{\Gamma}_\infty$; however, even in the case where the interfacial velocity is positive (i.e. the liquid at the interface is moving from left to right), the concentration of surfactant at $z = 0$ continuously increases with the instability. To disclose the mechanisms of mass transfer responsible for this increase, we analyze the evolution in time of each one of the four terms contributing to the equation of interfacial mass balance (Eq. (7)). This equation equates the time rate of change of the local concentration of surfactant (or local time variation LTV), which is the term on the left of Eq. (7), to the added contribution of the three terms appearing on the right; they correspond to the normal convection (NC), tangential convection (TC) and diffusion (D), respectively. For the system characterized by $\widetilde{\Gamma}_\infty = 25$ and $A = 0$, Fig. 8 depicts the values taken by these terms along the interface at each one of the five interfacial configurations already defined; Figs. 9 and 10 play a similar role for the other two more concentrated systems: $\widetilde{\Gamma}_\infty = 2.5$ and $\widetilde{\Gamma}_\infty = 1.3$, respectively.

Table 3
Axial component of the interfacial tangential force obtained from the values of T_{ns} shown in Fig. 6

Interfacial shape	F_z		
	$\widetilde{\Gamma}_\infty = 25$	$\widetilde{\Gamma}_\infty = 2.5$	$\widetilde{\Gamma}_\infty = 1.3$
(a)	4.9×10^{-3}	6.87×10^{-3}	1.18×10^{-2}
(b)	1.73	1.93	2.11
(c)	8.18	9.06	9.71
(d)	14.13	15.37	15.98
(e)	18.45	21.92	27.63

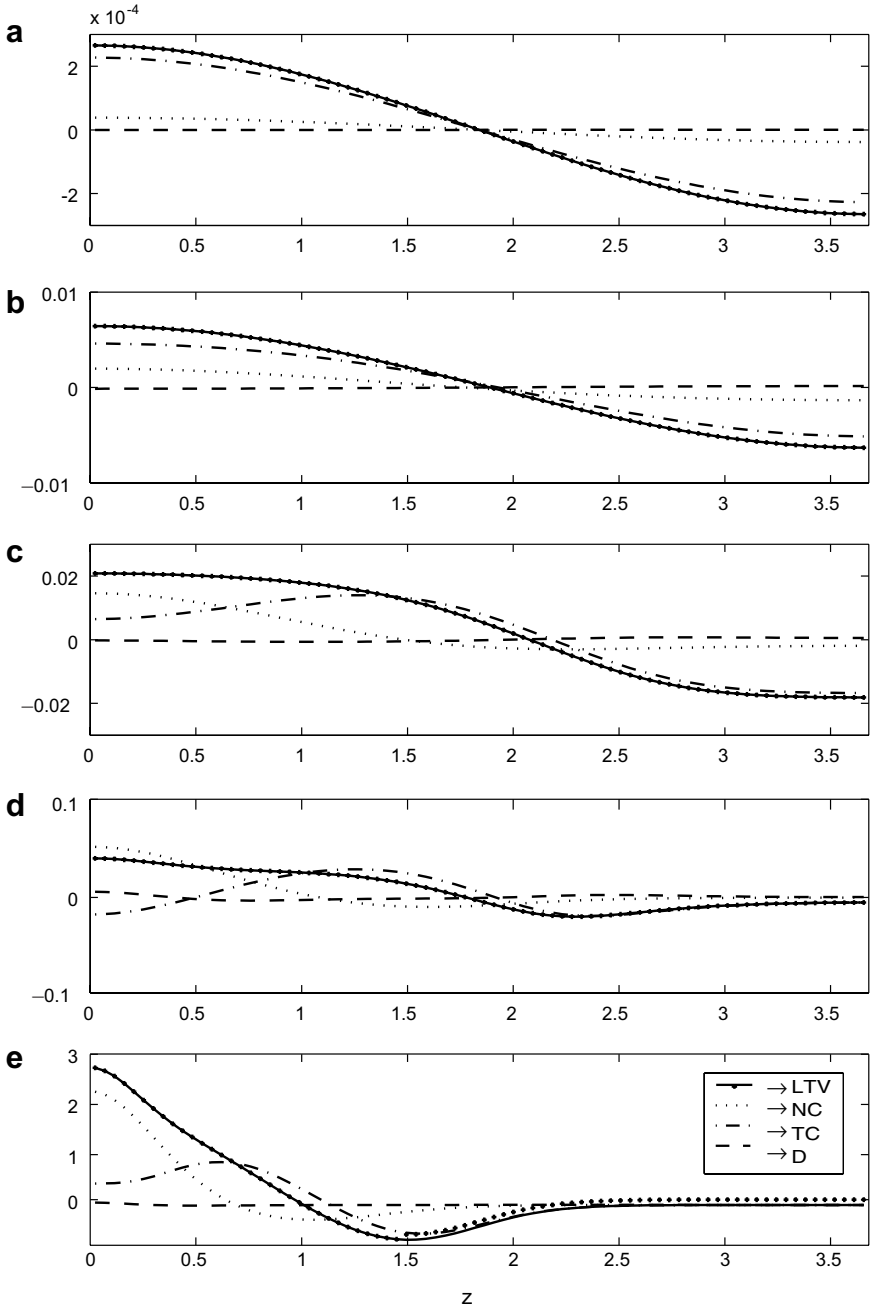

Fig. 8. Profiles of the four terms contributing to the interfacial mass balance (Eq. (7)) for the five interfacial configurations shown in Fig. 2. The system is the reference case with $A = 0$ and $\tilde{\Gamma}_\infty = 25$.

The results presented in Figs. 8–10 give evidence that normal convection always increases the concentration of surfactant in the zone where the liquid lobe develops; i.e. at, or close to $z = 0$. This occurs because the interfacial area shrinks as its radius becomes smaller and the adsorbed solute gets more concentrated; this mechanism is enhanced as the instability progresses. In addition, at the former steps of the process (configuration a) the tangential convection also carries solute in that direction for the three systems considered. Actually, at that time, this is the main mechanism by which the concentration of solute is augmented there. However, when

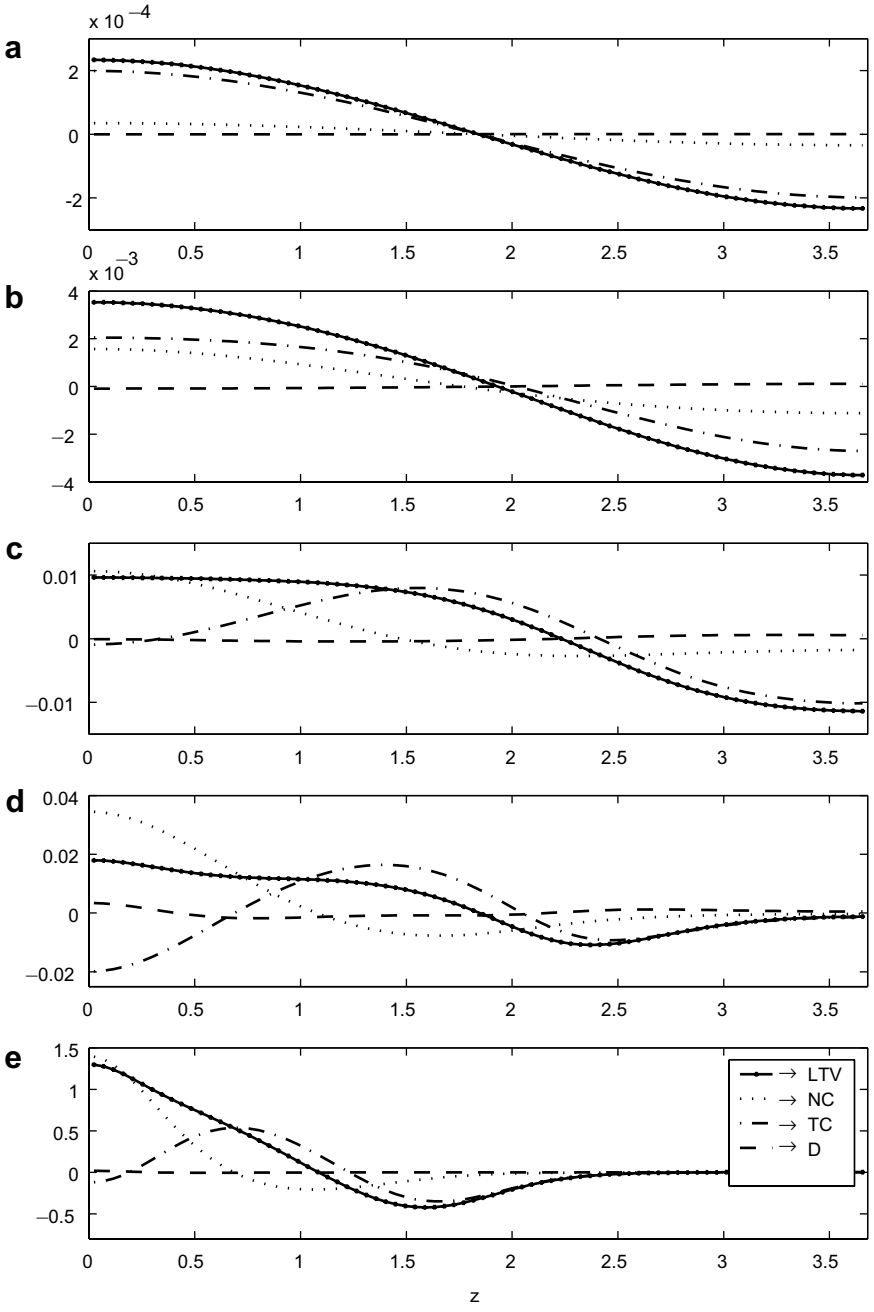

Fig. 9. As in Fig. 8 for $\widetilde{\Gamma}_{\infty} = 2.5$.

configuration b is reached, the tangential convection for the most concentrated system (Fig. 10) has just reversed direction and is now pulling solute out of the growing lobe. A similar phenomenon occurs for more advanced stages of the instability when the initial concentration is smaller (see Figs. 8 and 9).

The computed predictions presented above indicate that the effects of interfacial diffusion are almost negligible in all cases and at any stage of the process; therefore, for insoluble surfactants the time rate of change of the local concentration of solute is approximately given by interfacial convection. As the concentration of solute is increased, the mass transport by tangential convection increasingly opposes to the bulk flow motion retarding the unstable process; consequently, larger values of closure time are obtained.

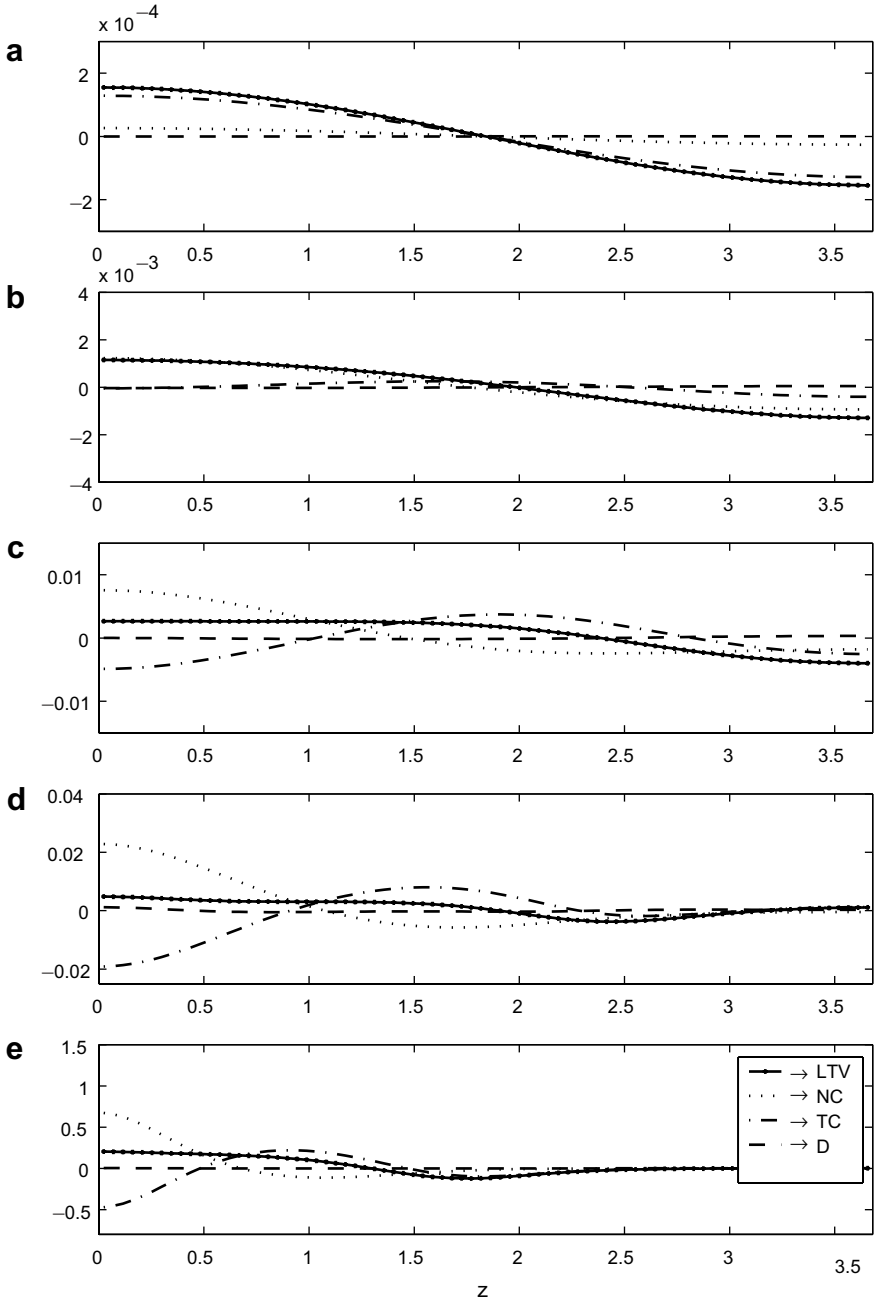

Fig. 10. As in Fig. 8 for $\widetilde{\Gamma}_\infty = 1.3$.

4.2. A non-ideal system ($A \neq 0$)

Results shown in Fig. 4 indicate that at any value of the initial concentration of surfactant, closure times increase as the interaction between the adsorbed molecules become more repulsive or, in other words, as the value of A decreases. According to our previous observations for an ideal solute ($A = 0$), we should expect larger closure times when the interfacial velocity presents a stronger opposition to the bulk flow motion. This expectation is confirmed when we examine the interfacial velocity profiles shown in Fig. 11 for systems with initial concentration of surfactant of 2.5 and values of A (from top to bottom) of 2, 0 and −2. It is clear that

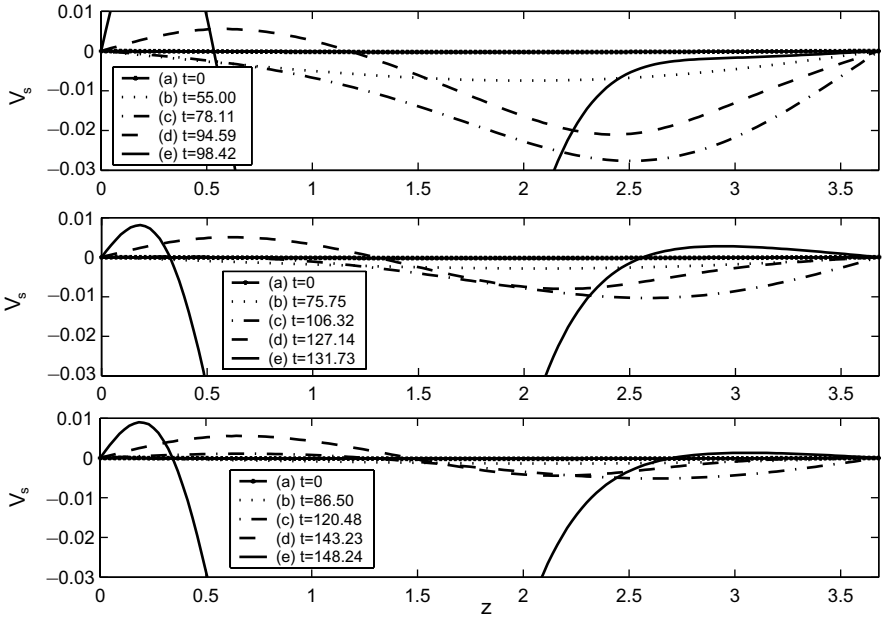

Fig. 11. Profiles of interfacial tangential velocities for the five interfacial configurations shown in Fig. 3. The system is the reference case with $\widetilde{\Gamma}_\infty = 2.5$; from top to bottom the values of A are 2, 0 and −2.

the tangential velocities carrying solute toward the lobe crest are larger for a solute with cohesive interactions ($A = 2$) than for an ideal solute ($A = 0$); thus, cohesive interactions result in a faster evolution of the instability as indicated by their respective dimensionless time. The opposite happens for a system containing solute with repulsive interactions: the tangential velocities portrayed at the bottom of Fig. 11 produce a stronger opposition to the bulk motion than the velocities portrayed at the center, and the instability is decelerated.

We have already argued that changes in tangential velocities should be related to Marangoni stresses and to the resulting tangential forces. In a similar way as we did in Table 3, in Table 4 we summarize the values of the axial component of the tangential force exercised on the interface; they result from integrating the T_{ns} profiles shown in Fig. 12, according to Eq. (20). As it was expected, at any stage of the instability from (a) to (d), the values increase from left to right; this is an indication that surfactants improve their stabilizing properties, and closure is attained at longer times as the molecular interactions become repulsive. At stage (e) the trend just described changes, and the largest force occurs for $A = 2$; this feature does not contradict the above conclusion since at this point the process of closure has already been triggered and the unstable evolution is not longer driven by capillary forces. In addition, the evolution becomes so fast that the crest of the lobe will reach the capillary axis almost instantaneously; this means that for practical purposes the closure time is determined by the previous stages (see Campana and Saita, 2006).

The results for closure times shown in this work present an interesting feature regarding the type of molecular interaction; Fig. 4 shows that for values of A smaller than one, closure times monotonically increase with the initial concentration of solute. However, for larger cohesive interactions, closure times not longer behave

Table 4
Axial component of the interfacial tangential force obtained from the values of T_{ns} shown in Fig. 12

Interfacial shape	F_z		
	$A = 2$	$A = 0$	$A = -2$
(a)	4.2×10^{-3}	6.87×10^{-3}	8.8×10^{-2}
(b)	1.62	1.93	2.04
(c)	7.94	9.06	9.42
(d)	14.48	15.37	15.62
(e)	23.04	21.92	22.25

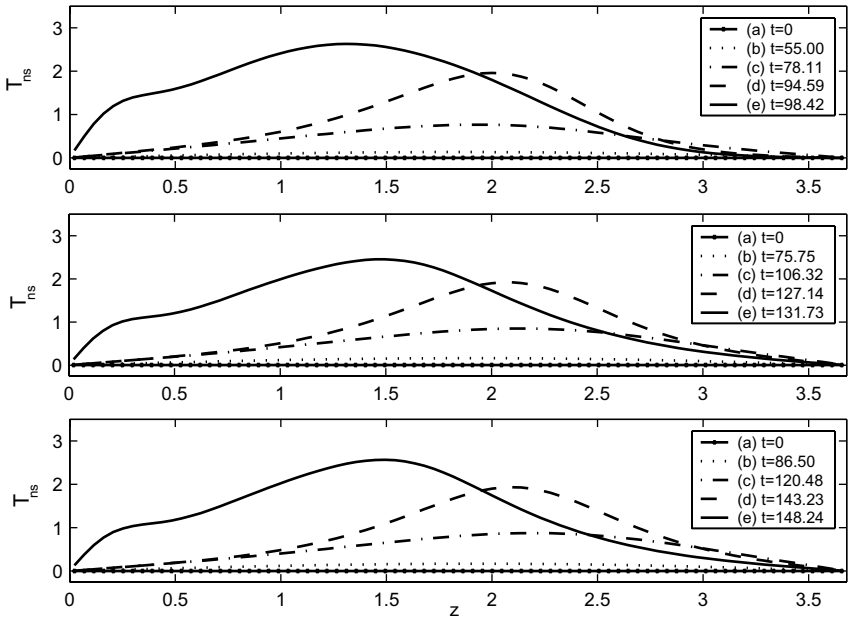

Fig. 12. Profiles of interfacial tangential stresses (as in Fig. 11).

Table 5
Axial component of the interfacial tangential force for different initial concentration of surfactant when $A = 2$

Interfacial shape	F_z		
	$\widetilde{\Gamma}_\infty = 25$	$\widetilde{\Gamma}_\infty = 2.5$	$\widetilde{\Gamma}_\infty = 1.3$
(a)	4.6×10^{-3}	4.2×10^{-3}	9.5×10^{-3}
(b)	1.69	1.62	2.05
(c)	7.97	7.94	9.56
(d)	13.78	14.48	16.12
(e)	17.76	23.04	29.48

in that way and they show a minimum for certain intermediate value of initial concentration; this trend is clearly exhibited in Fig. 4 when $A = 2$. As we mentioned before, closure times must be related to interfacial tangential stresses; thus, we resort again to the axial component of the tangential forces acting on the interface (F_z) to confirm that they vary accordingly.

Table 5 summarizes the values of F_z at the five configurations indicated in Fig. 3. For stages a–c the values indicate that the interfacial tangential forces slightly decrease when $\widetilde{\Gamma}_\infty$ is changed from 25 to 2.5; i.e. when the initial concentration of surfactant of a dilute system is increased. Since smaller tangential forces result in shorter evolution times, and considering that the time needed to reach stage c approximately constitutes 80% of the total evolution time, the closure time reduction occurring when $\widetilde{\Gamma}_\infty$ is changed from 25 to 2.5 and $A = 2$ (see Fig. 4), is explained.

We should point out that the just shown non-monotonic behavior is originated in the non-linear nature of the equation of state: if in Eq. (13) we differentiate E with respect to $\widetilde{\Gamma}_\infty$, is easy to show that an extreme is only possible when A is larger than one and that this extreme is a minimum. In agreement with the results presented in Table 5, the minimum value of E for $A = 2$ occurs when $\widetilde{\Gamma}_\infty = 3.41$.

4.3. Elastic parameter β

In order to determine how the elastic parameter affects the significance of the non-linear terms introduced with the equation of state, we computed closure times when β is 10 times greater than the value employed for the results shown in Fig. 4; the new results are depicted in Fig. 13.

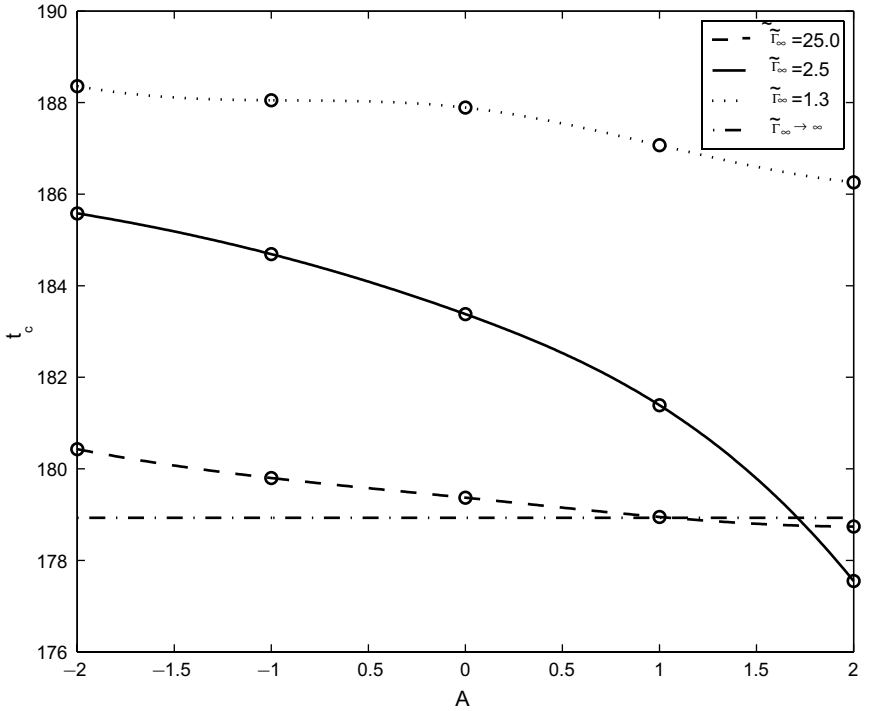

Fig. 13. Closure times versus A for different values of initial concentration. The parameters of the system are those of the reference case with $\beta = 0.1$; the closure time of the linear approximation is 178.93.

The curves of closure time in both figures look rather similar; i.e. the systems follow almost the same trend when $\widetilde{\Gamma}_\infty$ and A, are varied. However, it is evident that the relative changes produced either by $\widetilde{\Gamma}_\infty$ or by A are less significant when the value of β is larger. For example, if in Fig. 4 we compare closure times of the curve of $\widetilde{\Gamma}_\infty = 2.5$ with the constant closure time of the linear case, we observe relative differences ranging between 41.8% and –5.8% as we change A from -2 to 2. On the other hand, if we make a similar comparison with the closure times reported for $\beta = 0.1$ (see Fig. 13), we observe relative differences varying between 3.7% and –0.8%. We have also made the same comparison with closure times for $\beta = 1$ (not shown here) finding that the relative difference between the values for $\widetilde{\Gamma}_\infty = 2.5$ and the value pertaining to the linear case is less than 1% for any value of A in the interval -2, 2.

These results agree with those previously reported by Campana et al. (2004). In fact, when they studied the Rayleigh instability in capillaries under the presence of insoluble surfactants, they found that the curve of closure times versus β presents a rather steep S-shape connecting two plateau regions. The plateau region located at $\beta < 10^{-3}$ gives the minimum closure time, while the plateau region located at $\beta > 1$ gives the maximum closure time and also indicates that the elastic effects reach a saturation point near $\beta = 1$, i.e. they no longer increase beyond that point. Actually, for $\beta = 0.01$ they found a closure time increase of 45% of the time length separating both plateaus, while for β equal to 0.1 and 1 the increments were about 92% and 99%, respectively. It is evident that in the last two cases the changes in closure time that either $\widetilde{\Gamma}_\infty$ or A might produce are limited to small percentages, as occurs in the cases presented in Fig. 13.

5. Concluding remarks

In this work, we extended our previous analysis about the effects of insoluble surfactants on the Rayleigh instability in capillaries, by employing a more realistic surface equation of state that considers not only the initial amount of surfactant but also the interaction between adsorbed molecules. To examine in detail how

the interfacial variables and the mechanisms of interfacial transport of solute are affected, we changed parameters like initial concentrations, interaction between adsorbed molecules and surface elasticity.

We employed values of the elastic parameter (β) varying between 0.01 and 1; regardless of the value of β chosen, we found that closure times always behave according to the following pattern: (i) Repulsive interactions between adsorbed molecules produce larger closure times than ideal systems, while the opposite occurs with solutes interacting cohesively. (ii) The relative changes induced by molecular interaction depend on solute concentrations, being strong for intermediate concentrations and becoming less important for either dilutes or concentrated systems. (iii) In general, closure times increase with solute concentrations; but, if there exists an important cohesive interaction ($A > 1$), a non-monotonic behavior occurs and closure times first decrease and then increase as the concentration of solute is augmented.

We pointed out that the pattern just described does not depend on the surfactant strength; however, for the particular system analyzed in this work, the relative changes in closure time induced by molecular interactions or by surfactant concentrations, do depend on surfactant effectiveness. The results presented show that a strong insoluble surfactant produces a substantial reduction in the speed of the unstable process with a consequent increase in closure times. In this case, closure times are almost independent of both solute concentration and the existence of any kind of molecular interaction; i.e. closure times depend almost exclusively on the value of β and consequently, the employment of a linear surface equation of state should give results accurate enough.

On the other hand, for weaker surfactants, closure times depend strongly on the initial concentration of solute as well as on the type of molecular interactions. In this event, the use of an equation of state that consider the effects of theses variables should be appropriate since the results provided by a linear one might be rather questionable.

Though the foregoing conclusions are valid for the instability of thin films lining the inner walls of a capillary, they might also be valid when insoluble surfactants act on other unstable systems; further analyses are needed to confirm this presumption.

Acknowledgements

This work has been supported by funds granted by the Universidad Nacional del Litoral, CONICET and ANPCyT.

References

Campana, D.M., Di Paolo, J., Saita, F.A., 2004. A 2-D model of Rayleigh instability in capillary tubes. Surfactant effects. Int. J. Multiphase Flow 30, 431–454.

Campana, D.M., Saita, F.A., 2006. Numerical analysis of the Rayleigh instability in capillary tubes: the influence of surfactant solubility. Phys. Fluids 18, 1–16.

Chang, C-H., Franses, E.I., 1995. Adsorption dynamics of surfactants at the air/water interface: a critical review of mathematical models, data and mechanisms. Colloids Surf. A: Physicochem. Eng. Aspects 100, 1–45.

Edwards, D.A., Brenner, H., Wasan, D., 1991. Interfacial transport processes and rheology. In: Brenner, H. (Ed.), . In: Series in Chemical Engineering. Butterworth-Heinemann, Boston.

Gauglitz, P.A., Radke, C.J., 1988. An extended evolution equation for liquid film breakup in cylindrical capillaries. Chem. Eng. Sci. 43, 1457–1465.

Goren, S., 1962. The instability of an annular thread of fluid. J. Fluid Mech. 12, 309–319.

Halpern, D., Grotberg, J.B., 1993. Surfactant effects on fluid-elastic instabilities of liquid-lined flexible tubes: a model airway closure. J. Biomech. Eng. 115, 271–277.

Hammond, P.S., 1983. Nonlinear adjustment of a thin annular film of viscous fluid surrounding a thread of another within a circular cylindrical pipe. J. Fluid Mech. 137, 363–384.

Jensen, O.E., Grotberg, J.B., 1993. The spreading of heat or soluble surfactant along a thin liquid film. Phys. Fluids A 5, 58–68.

Kwak, S., Pozrikidis, C., 2001. Effect of surfactants on the instability of a liquid thread or annular layer – Part I: Quiescent fluids. Int. J. Multiphase Flow 27, 1–37.

Otis, D.R., Johnson, M., Pedley, T.J., Kamm, R.D., 1993. Role of pulmonary surfactant in airway closure: a computational study. J. Appl. Physiol. 75, 1323–1333.

Rayleigh, Lord., 1879. On the capillary phenomena in jets. Appendix I. Proc. Roy. Soc. A 29, 71–97.

Tomotika, S., 1935. On the instability of a cylindrical thread of a viscous liquid surrounded by another viscous liquid. Proc. Roy. Soc. A 150, 322–337.

Weber, C., 1931. Zum Zerfall cines Flüssigkeitsstrahles. Z. Angeur. Math. Mech. 11, 136–154.

Wong, H., Rumschitzki, D., Maldarelli, C., 1996. On the surfactant mass balance at a deforming fluid interface. Phys. Fluids 8, 3203–3204.

Wong, H., Rumschitzki, D., Maldarelli, C., 1999. Marangoni effects on the motion of an expanding or contracting bubble pinned at a submerged tube tip. J. Fluid Mech. 379, 279–302.